

Article

# Numerical Simulation of Transient Multiphase Flow in a Five-Strand Bloom Tundish during Ladle Change

Hua Zhang <sup>1</sup>, Ronghua Luo <sup>2</sup>, Qing Fang <sup>1</sup> , Hongwei Ni <sup>1,\*</sup> and Xiao Song <sup>1</sup>

<sup>1</sup> The State Key Laboratory of Refractories and Metallurgy, Wuhan University of Science and Technology, Wuhan 430081, China; huazhang@wust.edu.cn (H.Z.); qfang525@163.com (Q.F.); wscyxx@163.com (X.S.)

<sup>2</sup> Valin Xiangtan Iron and Steel Co., Ltd., Xiangtan 411101, China; luoronghua\_86@163.com

\* Correspondence: nihongwei@wust.edu.cn; Tel.: +86-027-6886-2811

Received: 30 December 2017; Accepted: 13 February 2018; Published: 23 February 2018

**Abstract:** The steel-slag-air multiphase flow in a bloom tundish with five strands during the transient casting of the ladle change was simulated using the Volume of Fluid (VOF) model, and the formation mechanisms of macro-inclusions and the behavior of the steel-slag-air interface during the filling process were investigated. Water model experiments were conducted to validate the multiphase model. The results showed that the numerical results of slag entrapment behavior and the exposed area of steel are basically consistent with the experimental results. The flow of molten steel in the tundish is weak except for the region around the stopper rods at the end of the emptying process. Strong fluctuations in liquid level were formed during the filling process, showing two wave crests in front of and behind the shroud in the impact zone, which intensified with the increase in filling time and then declined gradually. Entrapment phenomena and exposure of liquid steel could not be observed before the filling stage. While the entrapped slag droplets mostly float up and can be removed within 40 s during the filling process, the remainder enters the casting zone through the baffle. The maximum exposed area of molten steel is 252 cm<sup>2</sup> when the filling time is 4.0 s.

**Keywords:** tundish; ladle change; numerical simulation; multiphase VOF model; transient flow

## 1. Introduction

A transient casting process refers to a casting process in which the flow rates at the inflow and outflow differ (e.g., a ladle change) [1], and has become a key method for obtaining high-quality clean steel in continuous casting. Unfortunately, re-oxidation and the entrapment of slag during transient-state casting are much more serious issues than in steady-state casting, and lead to the number of billet quality defects being significantly higher [2,3]. The inlet/outlet conditions of the tundish change greatly during the ladle change period, leading the liquid level of the bath to rise and fall rapidly. The steel-slag interface fluctuations show instability, and the flow pattern changes significantly, meaning it has the apparent characteristics of transient flow. In particular, the ladle change operation between the previous and the next ladle of steady casting occurs repeatedly in a complete casting process, which is detrimental to overall quality control of continuous casting.

During the ladle change of the continuous casting process, minimizing the negative effects at the transient casting stage is a challenge faced by the world's metallurgists [4,5]. At present, most numerical investigations of the tundish have only considered the steady casting process using flow field modeling. Simulations of transient casting [6–13] are still only rarely undertaken. Takahashi et al. [7] simulated the velocity field in slab tundish during the ladle change, and provided a basis for predicting the change of the floating condition of inclusions. Bolling et al. [1] and Warzecha [8] studied the transient fluid flow and thermal distribution for a single-strand tundish by numerical simulation during the ladle change and steady-state casting. The Computational Fluid Dynamics (CFD) results

were verified using a water model experiment with Laser Doppler Anemometry (LDA) and Digital Particle Image Velocimetry (DPIV) measurements. Zhang et al. [4,9–11] studied fluid flow, heat transfer, and inclusion removal in a 2-strand 60 t slab tundish in the steady state and transient state by isothermal and non-isothermal numerical simulations. This study included cast start, sudden cast stop, ladle change, and the sudden closing of one strand, and gives us some valuable information on improving the cleanliness of molten steel. However, the liquid level fluctuation and the slag-gas two-phase behaviors in the bath were not considered. Fernandez et al. [12] calculated the steel-gas two-phase flow in an industrial tundish during grade transition casting by using a three-dimensional, unsteady Volume of Fluid (VOF) model. The changes in liquid level and flow field in the tundish during the ladle change were investigated. The simulation considered the relationship between the intermixed concentration distribution of steel and the duration of the filling stage, but the slag phase was ignored. At present, to the authors' knowledge, the understanding of transient flow in the tundish is still lacking. Investigations relating to steel-slag-air three-phase behaviors in simulations of multi-strand tundish during ladle change have rarely been reported.

The three-dimensional multiphase (air-slag-steel) flow during the ladle change process of a five-strand bloom tundish was simulated by a multiphase VOF model in this paper. The changes of flow field before and after the ladle change were investigated in order to deepen our understanding of the behavior of the air-slag-steel interface, and provide a theoretical basis for adjusting the transient-state casting operation and improving the quality of the billet. Additionally, water model experiments of slag entrapment behavior and the exposed area of steel in the impact zone were conducted and computed to validate the numerical multiphase model.

## 2. Model Descriptions

### 2.1. Basic Assumptions

The actual fluid flow in a tundish is a complicated physical and chemical process. The principal assumptions made in the modeling of the transient fluid flow during the ladle change are as follows:

- (1) There are no chemical reactions among the phases in a molten bath;
- (2) The cover slag is regarded completely as a liquid in the tundish;
- (3) Air, slag and molten steel are treated as incompressible viscous fluids with the fixed physical properties;
- (4) There is no slip and interpenetration among the fluids;
- (5) The influence of temperature on the flow field in the tundish is ignored.

### 2.2. Governing Equations

In order to accurately investigate the dynamic behavior of the three phases flow in the tundish during the ladle change, a multiphase VOF model is applied to calculate the behavior of the steel-slag-air interfaces. Since a void region is not allowed in this model, the volume fractions of all phases sum to unity in each control volume.

$$\sum_{i=1}^n \alpha_i = \alpha_{air} + \alpha_{slag} + \alpha_{steel} = 1 \quad (1)$$

The fields for all variables and properties are shared by the phases and represent volume-averaged values, as long as the volume fraction of each of the phases is known at each location. Thus, the volume fraction average properties in any given control cell are computed in the following form, such as for volume fraction average density ( $\rho_m$ ) and viscosity ( $\mu_m$ ):

$$\rho_m = \sum_{i=1}^n \alpha_i \rho_i, \quad \mu_m = \sum_{i=1}^n \alpha_i \mu_i \quad (2)$$

where  $\alpha_i$  and  $\rho_i$  are the volume fraction and density of phase  $i$ , respectively.

(1) The multiphase VOF model [1] can be expressed as follows:

Continuity equation:

$$\frac{1}{\rho_i} \left[ \frac{\partial}{\partial t} (\alpha_i \rho_i) + \nabla \cdot (\alpha_i \rho_i \vec{v}_m) \right] = \sum_{i=1}^n (m_{ij}^{\rightarrow} - m_{ji}^{\rightarrow}) \quad (3)$$

where  $m_{ij}^{\rightarrow}$  is the mass of phase  $i$  flow into phase  $j$ ; and  $m_{ji}^{\rightarrow}$  is the mass of phase  $j$  flow into phase  $i$ ,  $\vec{v}_m$  is the velocity of mixture.

Momentum equation:

$$\frac{\partial (\rho_m \vec{v}_m)}{\partial t} + \nabla \cdot (\rho_m \vec{v}_m \vec{v}_m) = -\nabla p + \nabla [\mu_m (\nabla \vec{v}_m + \nabla \vec{v}_m^T)] + \rho_m \vec{g} + \vec{F} \quad (4)$$

where  $\vec{F}$  is the surface tension force item:

$$\vec{F} = 2\sigma_t \rho_m k_i \nabla \alpha_i / \sum_{i=1}^n \rho_i \quad (5)$$

where  $\sigma_t$  is the surface tension coefficient, and  $k_i$  is the curvature, the surface tension coefficient value between steel and slag is 1.4.

(2) The fluid flow in the tundish is a complicated turbulent flow, and turbulence modeling is expressed through the standard  $k$ - $\varepsilon$  model.

Turbulence kinetic energy equation:

$$\frac{\partial (\rho_m k)}{\partial t} + \nabla \cdot (\rho_m \vec{v}_m k) = \nabla \cdot \left( \frac{\mu_{t,m}}{\sigma_k} \nabla k \right) + G_{k,m} - \rho_m \varepsilon \quad (6)$$

Rate of dissipation equation:

$$\frac{\partial (\rho_m \varepsilon)}{\partial t} + \nabla \cdot (\rho_m \vec{v}_m \varepsilon) = \nabla \cdot \left( \frac{\mu_{t,m}}{\sigma_\varepsilon} \nabla \varepsilon \right) + \frac{\varepsilon}{k} (C_{1,s} G_{k,s} - c_{2,s} \rho_m \varepsilon) \quad (7)$$

In these equations, the effective viscosity  $\mu_{t,m}$  and the generation of turbulence energy  $G_{k,m}$  can be calculated as follows:

$$\mu_{t,m} = \mu_m + \mu_t = \mu_m + \frac{\rho_m c_\mu k^2}{\varepsilon}, \quad G_{k,m} = \mu_t \nabla \vec{v}_m (\nabla \vec{v}_m + \nabla \vec{v}_m^T) \quad (8)$$

where  $C_{1,s}$ ,  $c_{2,s}$ ,  $c_\mu$ ,  $\sigma_k$  and  $\sigma_\varepsilon$  are the empirical constants of the  $k$ - $\varepsilon$  model. The values of these constants are 1.43, 1.92, 0.09, 1.0 and 1.3, respectively;  $\mu_t$  is the turbulent viscosity.

### 2.3. Boundary Conditions

The transient casting of the ladle change in the tundish can be divided into two processes (Figure 1), in which the  $W_{\text{tundish}}$  is the weight of liquid steel, and the  $Q_{\text{steady}}$  ( $2.66 \times 10^{-3} \text{ m}^3/\text{s}$ ) refers to the flow rate of liquid steel at steady state. The first process involved the level of molten steel dropping at the emptying stage when the slide gate of the ladle was closed. The second involved the liquid level rising during the filling process while the slide gate was open.

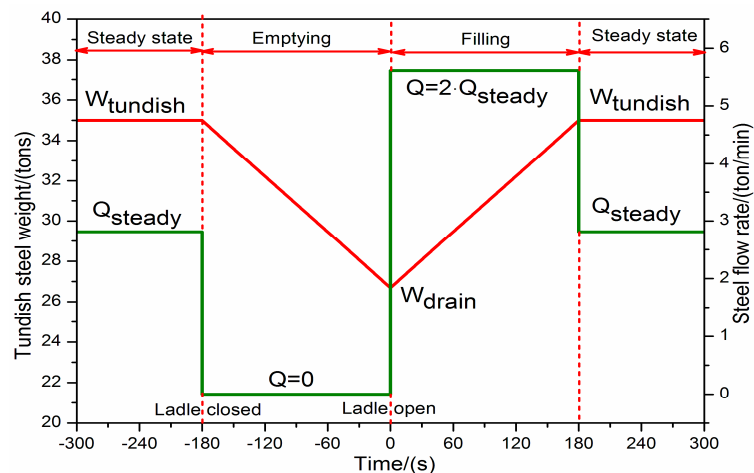


Figure 1. Process diagram of the ladle change in the tundish.

According to actual fluid flow in the tundish, the boundary conditions of the model can be determined as follows:

(1) The shroud was given the pressure-inlet in the emptying process and velocity-inlet in the filling process, respectively. The boundary values for  $k$  and  $\varepsilon$  at the inlet were calculated as  $k = 0.01 u_{inlet}^2$ ,  $\varepsilon = 2k^{1.5}/d_{inlet}$ , where the  $u_{inlet}$  and  $d_{inlet}$  are the velocity and diameter of computational inlet.

(2) The outlet of the tundish was set as the velocity-outlet, and the velocity could be calculated from the casting speed and section size.

(3) The top surface of the tundish was used as the pressure-inlet, and standard atmospheric pressure was chosen for the pressure value.

(4) The horizontal components of the velocity and horizontal gradient of all the gradients of the symmetry plane were set at zero.

(5) The solid wall of the tundish was considered a no-slip boundary condition and the near-wall region was treated as a standard wall function.

#### 2.4. Numerical Method

A three-dimensional mathematical model was established according to the real size of the industrial tundish (Figure 2), and considering the symmetry of the tundish, half of the real tundish was taken as the computational domain. The main process parameters of the continuous caster are listed in Table 1. After the shroud was inserted into the molten bath, a layer of slag would float on the liquid level and the air would fill up the rest of the space in the shroud before opening the ladle slide gate in the ladle change process. To truly model the ladle change process, the solution initialization of the model took into consideration that the slag layer and air column existed in the shroud, as shown in Figure 3.

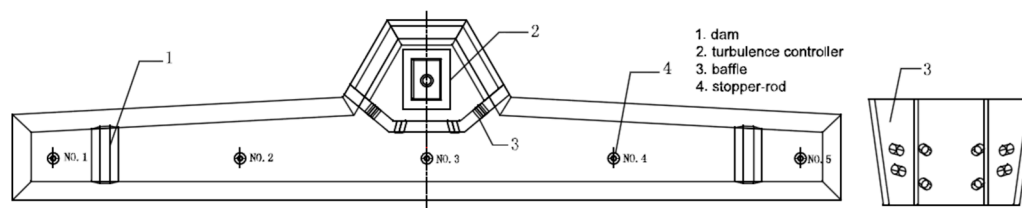


Figure 2. Configuration of the industrial tundish.

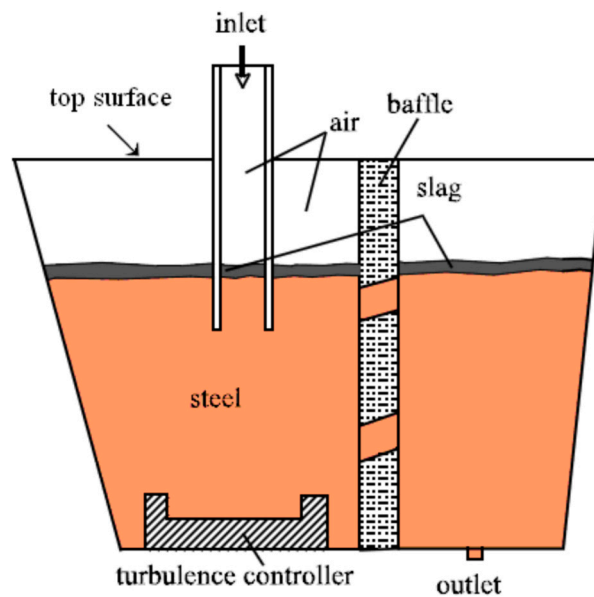
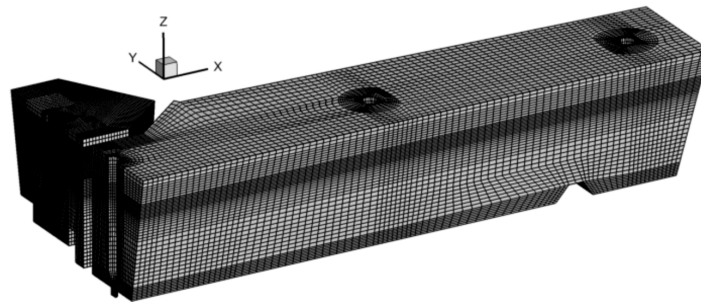


Figure 3. Schematic of solution initialization during the ladle change.

Table 1. Main process parameters.

Casting Condition	Value
Working capacity of tundish, t	35
Bloom cross section, mm <sup>2</sup>	280 × 380
Casting speed, m/min	0.63
Height of molten steel, mm	800
Inner diameter of nozzle, mm	81
Submergence depth of nozzle, mm	310
Thickness of slag layer, mm	40

The mathematical model was solved by CFD commercial software FLUENT 12.1 (Ansys Inc., Canonsburg, PA, USA). The PISO (Pressure Implicit with Splitting of Operators) algorithm was used for coupling the pressure and velocity terms. Additionally, the interface of fluids was tracked by the Geo-reconstruct method [14]. To simulate the behavior of the steel-slag-air interface and impact zone more accurately, local grid refinement technology was applied, and the meshes of the FLUENT computational domain included non-uniform grids with about 300,000 cells, as shown in Figure 4. Simultaneously, mesh refinement of the steel-slag interface was considered. Under the precondition of unchanged casting speed, the time of the ladle change was 3 min from the gate closing in the last heat to the gate opening in the next heat. The flow field at the end of emptying process was the initial period of the filling process, and the steel flow rate of the shroud was 2 times that of normal steady-state casting. The convergence criterion was established when the sum of all residuals for the dependent variable is less than  $10^{-4}$ . Moreover, the under relaxation factors of moment, pressure,  $k$ ,  $\varepsilon$  and energy were reduced to values between 0.2 and 0.6 to improve the convergence history. A typical calculation for the simulation of 360 s, with the conditions of the starting zero velocity field and a time step of 0.005 s, required 600 h computational time using an Intel Core i5 CPU 2.8 GHz with 4.00 GB of RAM. The physical parameters of the fluids used for the transient simulation are presented in Table 2.



**Figure 4.** Computational mesh.

**Table 2.** Physical parameters of fluid used in simulation.

Property	Air	Slag	Steel
Density, kg/m <sup>3</sup>	1.225	2700	7000
Viscosity, pa·s	$1.79 \times 10^{-5}$	0.6	0.0065

### 3. Results and Discussion

#### 3.1. Model Validations

The simulation results of the multiphase flow field were verified by the 1:3 water model experiments. Detailed information about the equipment used for the water model experiments can be found elsewhere [15]. The vacuum pump oil in yellow on the top of the water model was used to represent the slag phase. The Froude (Fr) and Weber (We) criteria are suitable for investigations of surface waves and interaction of interfaces, in which the real Froude and Weber numbers are equal to the Froude and Weber numbers of the water model [16]. The ratio of flow velocity, flow rate, and duration of time between the water model and numerical model were calculated to be 0.577, 0.06145 and 0.577, respectively, based on the geometric ratio and similarity number. The exposed area of steel in the impact zone and slag entrapment was filmed and calculated to validate the simulation results. Figure 5 shows the comparison of the simulation and the experimental results of slag entrapment at 1.3 s (a) and the exposed area of steel in the impact zone at 12 s (b), respectively, in which the dark blue areas in the left of Figure 5a,b represent the slag phase; the color change of the slag phase means a change of slag volume fraction. Table 3 lists the statistical comparisons between the exposed area of steel in the impact zone and the numerical and experimental results at different moments. It can be seen from Figure 5 and Table 3 that the simulated results of slag entrapment behavior and the exposed area of steel are basically consistent with the experimental results, and the errors of the computed exposed area of steel in the impact zone by the numerical model at different moments are within 5% of the experimental results.

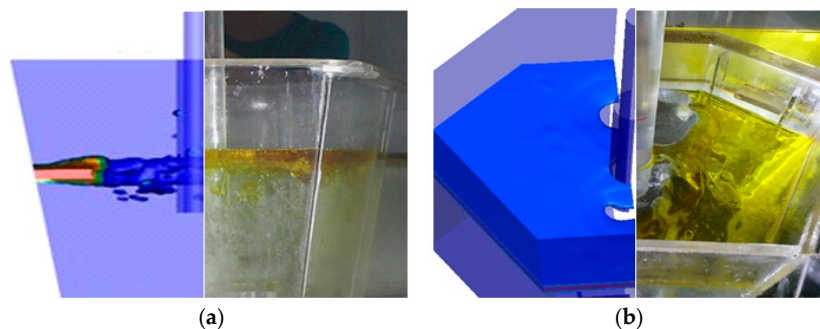


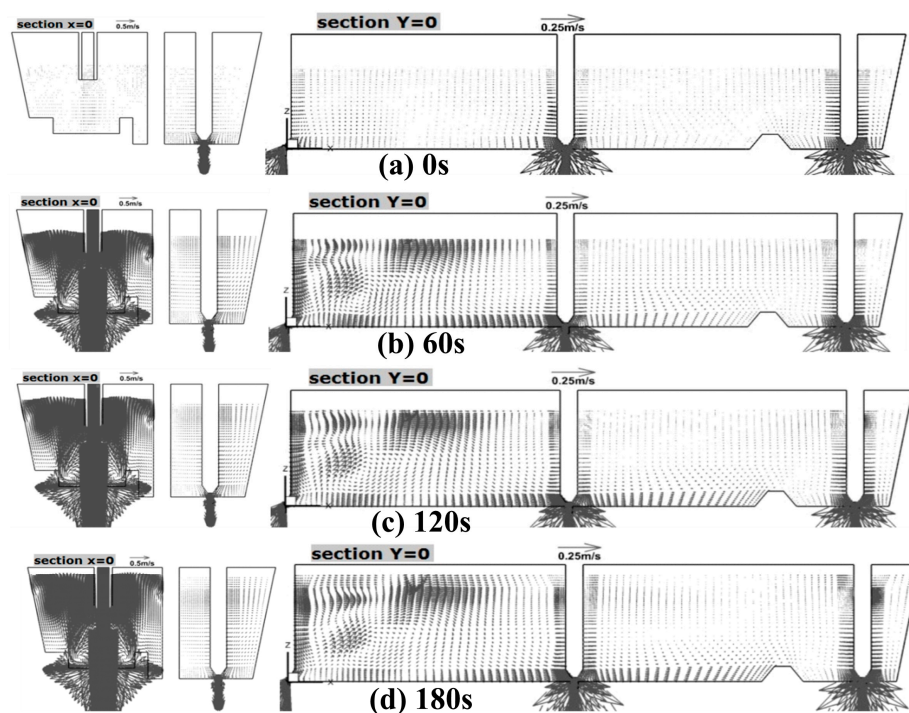
**Figure 5.** Comparison of the simulation and experimental results of slag entrapment at 1.3 s (a) and the exposed area of steel in the impact zone at 12 s (b).

**Table 3.** Statistical comparison of the numerical and experimental results of the exposed area of steel in the impact zone.

Time, s	Numerical Results, cm <sup>2</sup>	Experimental Results, cm <sup>2</sup>	Errors, %
1.3	167	174	4.2
5	188	197	4.6
20	163	168	3.0

### 3.2. The Flow Field of Molten Steel in the Tundish

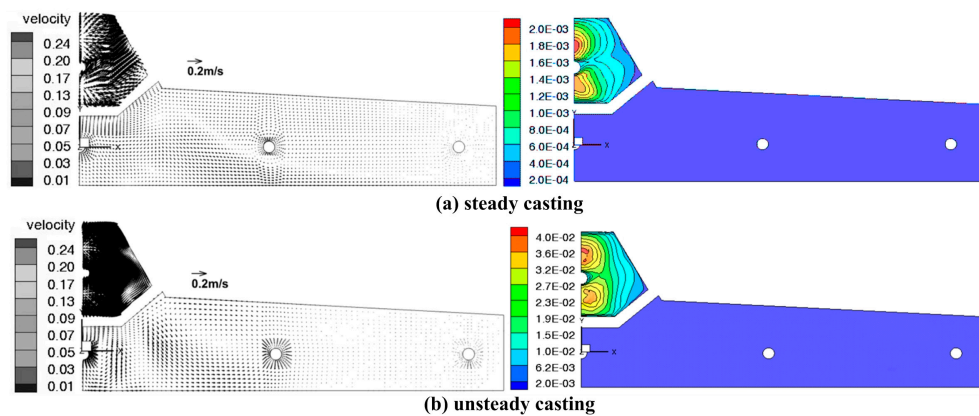
The variation of the steel flow field in the tundish is shown in Figure 6. Figure 6a shows the flow field of molten steel at an emptying time of 3.0 min (filling time of 0 s), which suggests that the liquid level dropped to the lowest position, and the molten steel flow was very weak throughout the whole tundish, except around the region of the stopper rods. From Figure 6a–d, it can be seen that the molten steel flow in the tundish was strengthened, apparently because of the steel jets stirring at high speed during the filling process. In particular, the flow speed of the impact zone is higher. As the filling time increased, the stronger flow volume of the molten steel continued to expand and the liquid level rose dramatically. The “dead zone” in the tundish had almost disappeared by the end of the filling time (180.0 s), and the liquid surface returned to approximately the steady casting height, as shown in Figure 6d.



**Figure 6.** Change of the steel flow field before and after the filling of the tundish. (a) 0 s; (b) 60 s; (c) 120 s; (d) 180 s.

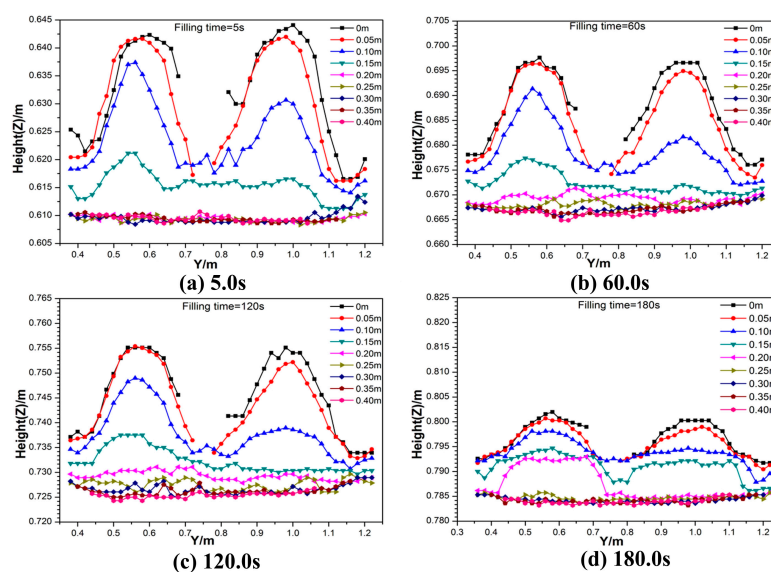
Figure 7 shows the velocity vector (left) and the turbulent kinetic energy distribution (right) of the molten steel level in steady and unsteady casting (with a filling time of 60 s), which was calculated using the standard  $k-\epsilon$  model. The steel flow of the surface in the impact zone is obviously stronger than that in the casting zone, and the turbulent kinetic energy is higher in the impact zone. Simultaneously, the molten steel flow is stable and uniform in the casting zone close to the baffle, but it is too slow on both sides of the tundish. In transient casting, during the filling process, the steel level flow in the tundish is obviously stronger than in steady-state casting, and the highest velocity exceeds 0.24 m/s in

the impact zone. Additionally, the turbulent kinetic energy reaches the maximum value of  $0.04 \text{ m}^2/\text{s}^2$ , which is much higher than that of the steady casting ( $0.002 \text{ m}^2/\text{s}^2$ ). The reason for this is that the molten steel in the impact zone achieves a greater stirring power under the impact of the steel jet from the ladle during the filling process, which causes the molten surface to fluctuate at different levels. Then, the steel-slag interface in the impact zone is in a continuously unsteady state, which can easily lead to entrapment and steel re-oxidation. Therefore, the steel level fluctuations cannot be neglected in the impact zone during the transient casting process.



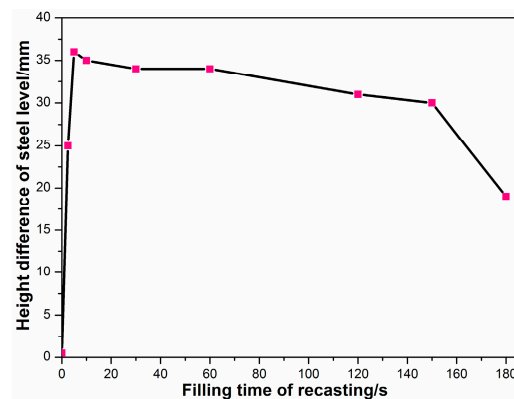
**Figure 7.** Velocity vectors and the turbulent kinetic energy distribution of the molten steel level in steady and unsteady casting (filling time of 60 s): (a) steady casting; (b) unsteady casting.

Figure 8a–d shows the steel level fluctuations of the  $x$ -direction section in the impact zone at filling times of 5.0 s, 60.0 s, 120.0 s, and 180.0 s, respectively. Two wave crests in the molten surface about 0.2 m away from the front and back of the shroud in the impact zone can be seen, and the fluctuation of the symmetry plane (section  $x = 0$ ) is the largest and highest in the impact zone. As the  $x$  coordinate increases, the fluctuation of the steel level decreases gradually, and the wave crests disappear when the section is beyond  $x = 0.25 \text{ m}$ . As the filling time increases, the height of the liquid level rises gradually, but the fluctuation range decreases gradually in the impact zone. Simultaneously, the area of the fluctuation region first increases and then decreases in the impact zone as time increases, as shown in Figure 8.



**Figure 8.** Level fluctuation of the  $x$ -axis sections with different filling times in the impact zone. (a) 5.0 s; (b) 60.0 s; (c) 120.0 s; (d) 180.0 s.

The fluctuation of the molten surface in the impact zone during the filling process is shown in Figure 9. In the early stage of the filling process, due to the steel jet strongly impacting on the tundish, the fluctuation range in the impact zone rises sharply, and reaches the maximum of 36 mm at a filling time of 5.0 s. Thereafter, the fluctuation range in the impact zone begins to drop, but the change is not obvious at filling times between 5.0 s and 150.0 s, with a minute drop of 5 mm. When the filling time exceeds 150.0 s, the fluctuation of the molten surface declines more quickly, and it drops to 19 mm at the end of the filling process.



**Figure 9.** Height difference with filling time of the steel level in the impact zone.

Based on the analysis above, the flowing state of molten steel in the tundish varies obviously during the ladle change, reflecting a classical transient flow. In particular, the speed variation is faster and the fluctuation range of the molten surface is greater in the impact zone, both before and after the filling period, than that of steady-state casting. These flow patterns will cause the slag or air to be entrapped in the molten steel in the impact zone. Additionally, it may cause the exposure of molten steel if the slag layer is broken by the strong impact. Therefore, it is necessary to analyze the interface behaviors of the steel-slag-air three-phase to get further information on the filling process.

### 3.3. Steel-Slag-Air Multiphase Behavior

The air distribution in the molten bath of the impact zone is shown in Figure 10. It can be seen that the air in the shroud is brought into the molten bath by the steel jet after opening the shroud. Due to the effect of the buoyancy force, most of the gas breaks away from the steel jet and quickly floats around the shroud. Then, most of the gas escapes to the atmosphere through the slag layer, and the rest of the gas disperses in the molten bath as smaller bubbles. With the large difference in density between the air and the steel, the bubbles remaining in the molten steel can be almost entirely removed within 4.0 s during the filling period, as shown in Figure 10d.

The distribution of slag in the tundish during the filling process is shown in Figure 11. Figure 11a shows that the interface of the steel-slag is smooth and stable, and there isn't the phenomenon of steel-slag entrapment or molten steel exposure before re-filling casting (the filling time). Figure 11b shows that the slag in the nozzle is brought into the molten bath by the steel jet, impacting at the beginning of the filling stage. Then the slag is broken up into lots of slag droplets distributed through the molten steel, as illustrated in Figure 11c, arrow 1. Since there is a smaller difference in density between the slag and molten steel, the entrapped slag droplets are hardly reduced at all in a short time period, even though some of the droplets are brought into the casting zone through the diversion hole of the baffle, as shown by arrow 3 of Figure 11c. It is far more likely that droplets of small size will become entrapped in the mold and form macro-inclusions. Figure 11d shows that slag droplets of larger size are almost all removed within 40.0 s of the filling process and just a few smaller droplets remained in the bath.

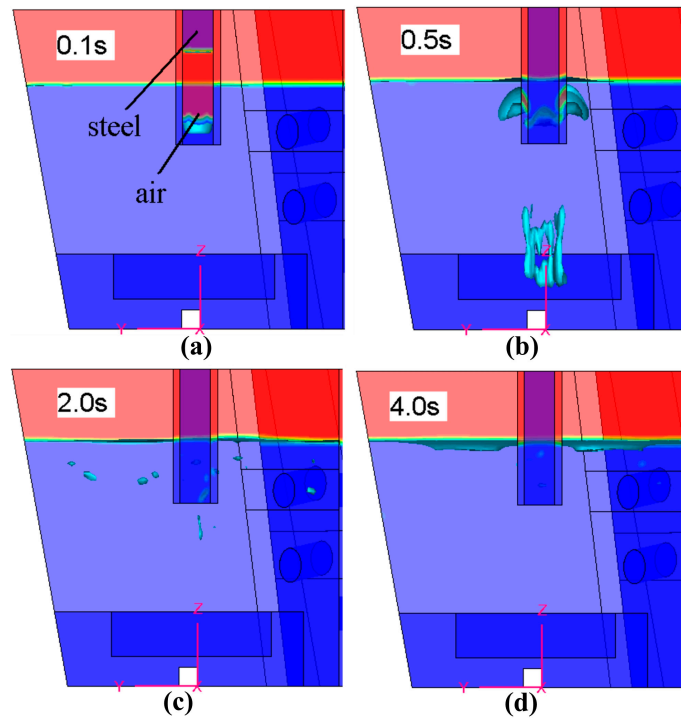


**Figure 10.** Air distribution in liquid steel at the beginning of recasting. (a) 0.1 s; (b) 0.5 s; (c) 2.0 s; (d) 4.0 s.

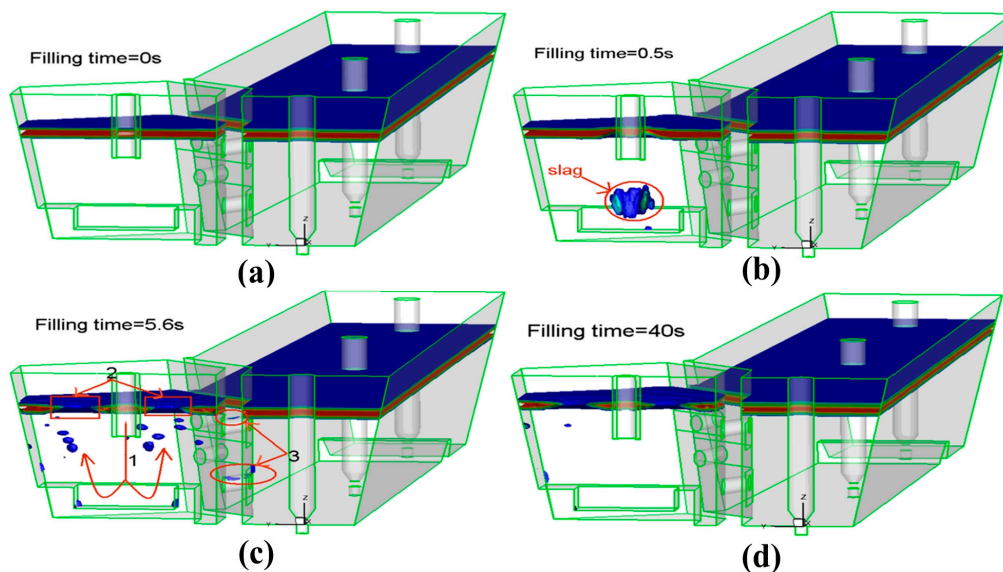


**Figure 11.** Slag distribution in the tundish bath. (a) 0 s; (b) 0.5 s; (c) 5.6 s; (d) 40 s.

During the filling process, the nozzle jet from the ladle is rebounded and forms up-stream, while the jet reaches to the bottom of the turbulence controller. After that, two wave crests are formed in front of and behind the nozzle in the impact zone, which are caused by the impingement of the up-stream. Finally, the molten steel spreads around to a surface flow. Therefore, the cover slag layer is pushed open, and the molten steel is exposed due to the intense impact of the up-stream and the strong shear stress of the surface flow in the impact zone (as shown by arrow 2 in Figure 11c). The distribution of the slag layer in the impact zone at filling times of 0.8 s and 120.0 s are shown in Figure 12.

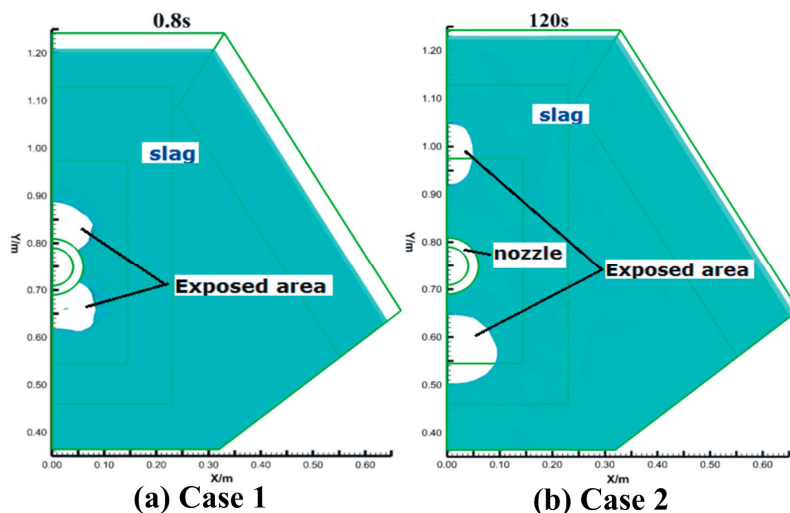


Figure 12. Slag layer shape in the impact zone.

According to the behaviors of the steel-slag-air three-phases at different times, illustrated in Figures 10 and 11, molten steel exposure in the impact zone is divided into two cases. In the first case, it is distributed mainly around the nozzle wall, which is caused by the gas brought through the slag layer in the beginning of the filling process, as shown in Figures 10b and 12a. In the second case, it is distributed in the area in the front and back of the nozzle, which is due to the intense impact of the up-stream and the strong shear stress of the surface flow during the filling process, as shown in Figures 11c and 12b.

Based on the statistics of the area of the exposed region during the filling time, the relationship between the area of the exposed region and time in the two cases above is shown in Figure 13.

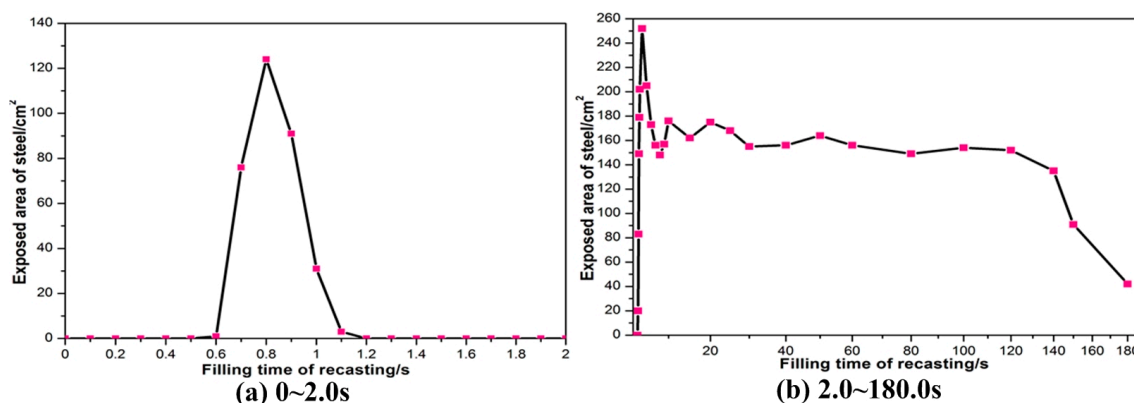


Figure 13. The exposed area with the filling time. (a) 0~2.0 s; (b) 2.0~180 s.

For the bubbles floating up through the slag layer, the exposure of the molten steel in case one begins appearing at a filling time of 0.5 s, and reaches its maximum area of  $124 \text{ cm}^2$  at 0.8 s, as presented in Figure 13a. The duration of the exposure remained at 0.6 s for the air passing through slag layer quickly, so the influence on re-oxidation can be ignored. Figure 13b shows that in case two, the exposure begins at a filling time of 3.0 s, and the exposed area increases quickly, reaches a maximum of  $252 \text{ cm}^2$ , and then declines quickly to  $173 \text{ cm}^2$  at a time of 6.0 s. Between the times of 6.0 s and 120.0 s, the exposed area remains steady in the range from 148 to  $176 \text{ cm}^2$ . After the filling time goes beyond 120.0 s, the exposed area apparently decreases to  $42 \text{ cm}^2$  at 180.0 s. The reason for such a phenomenon is related to up-stream resistance. With the increase of casting time and depth of the molten bath, the resistance of the up-stream increases gradually, the fluctuation range of the

steel levels, and the velocity of the surface flow declines. Thus, the impact force and the horizontal shearing stress declined accordingly, which leads to the slag layer gradually closing up.

According to the analysis above, the fluid flow is a transient state in the tundish during the ladle change. The strong impact of the steel jet, steel/air entrapment, steel/slag entrapment and the exposure of molten steel occurring in the impact zone lead to quality defects of the billet that are more serious than those occurring in steady-state casting.

To investigate the effect of secondary cooling types on the temperature field more specifically, the solidification process and structure in the continuous casting bloom, and the numerical results of the heat transfer and structure under the two cases mentioned above, are discussed and compared statistically.

#### 4. Conclusions

This work investigated the transient fluid flow phenomena in a five-strand bloom tundish during the ladle change of the continuous casting process. A three-dimensional mathematical model was developed with VOF to track the interface between different phases in the transient casting period. The main conclusions can be summarized as follows:

(1) The simulated results of slag entrapment and the exposed area of steel in the impact zone are basically consistent with water model experiments. The VOF model is suitable for modeling the multiphase flow in tundish. The changing character of flow and the steel-slag-air phase's interface behaviors can be predicted by numerical simulation during the ladle change process.

(2) At the end of emptying process, the molten steel flow is very weak except in the region around the stopper rods in the tundish. However, during the filling process, the molten steel flows and stirs strongly, and the liquid level fluctuates obviously, with two wave crests in the front of and behind the shroud in the impact zone. As the filling time increases, the fluctuation area expands, and the range increases rapidly before later declining gradually.

(3) The steel-slag interface is stable, and entrapment between different phases was not observed before the filling stage. However, it was found that slag entrapment occurred between steel and slag, between steel and air, and at the exposure area of steel. Most of the entrapped slag droplets rise up to be removed within 40 s and small parts enter into the casting area through the baffle. In addition, the area of molten steel exposed to air reaches its maximum value of about 252 cm<sup>2</sup> at a filling time of 4.0 s, and then gradually declines.

**Acknowledgments:** The authors would like to express their gratitude for the financial support by the National Natural Science Foundation of China No. 51471122, 51604200 and 51774217.

**Author Contributions:** Hongwei Ni and Hua Zhang conceived and designed the study. Ronghua Luo performed the experiments and simulations. Hua Zhang and Qing Fang contributed to the result analysis and paper preparation. Ronghua Luo and Xiao Song wrote the manuscript.

**Conflicts of Interest:** The authors declare no conflict of interest.

#### References

1. Bolling, R.; Odenthal, H.; Pfeifer, H. Transient fluid flow in a continuous casting tundish during ladle change and steady-state casting. *Steel Res. Int.* **2005**, *76*, 71–80. [[CrossRef](#)]
2. Sahai, Y. Tundish technology for casting clean steel: A review. *Metall. Mater. Trans. B* **2016**, *47*, 2095–2106. [[CrossRef](#)]
3. Liu, Z.; Li, B.; Zhang, L.; Xu, G. Analysis of transient transport and entrapment of particle in continuous casting mold. *ISIJ Int.* **2014**, *54*, 2324–2333. [[CrossRef](#)]
4. Ling, H.; Zhang, L. Numerical simulation of the growth and removal of inclusions in the molten steel of a two-strand tundish. *JOM* **2013**, *65*, 1155–1163. [[CrossRef](#)]
5. Cho, S.M.; Kim, S.H.; Thomas, B.G. Transient fluid flow during steady continuous casting of steel slabs: Part I. Measurements and modeling of two-phase flow. *ISIJ Int.* **2014**, *54*, 845–854. [[CrossRef](#)]

6. Alaei, A.R.; Edris, H.; Shirani, E. Upward molten flow for optimization of fluid flow in continuous casting tundish. *J. Iron Steel Res. Int.* **2010**, *17*, 34–39. [[CrossRef](#)]
7. Takahashi, K.; Ando, M.; Ishii, T. Numerical investigation of unsteady molten steel flow and inclusion behavior in the tundish in the ladle change period. *ISIJ Int.* **2014**, *54*, 304–310. [[CrossRef](#)]
8. Warzecha, M. Numerical and physical modelling of steel flow in a one-strand continuous casting tundish. *Metallurgija* **2011**, *50*, 147–150.
9. Zhang, L. Transient fluid flow phenomena in continuous casting tundishes. *Iron Steel Technol.* **2010**, *7*, 55–69.
10. Ling, H.; Zhang, L.; Li, H. Mathematical modeling on the growth and removal of non-metallic inclusions in the molten steel in a two-strand continuous casting tundish. *Metall. Mater. Trans. B* **2016**, *47*, 2991–3012. [[CrossRef](#)]
11. Ling, H.; Zhang, L.; Wang, H. Effect of different removal conditions on the growth and removal of inclusions in the molten steel in a two-strand tundish. *Metall. Res. Technol.* **2017**, *114*, 516. [[CrossRef](#)]
12. Fernandez, J.M.O.; Morros, C.S.; Somoano, J.R.; Ordieres, M.A. Multiphase modelling of the steel grade transition in a continuous casting tundish. In Proceedings of the ASME 2009 Fluids Engineering Division Summer Meeting, Vail, CO, USA, 2–6 August 2009; pp. 2183–2194.
13. Siddiqui, M.I.H.; Jha, P.K. Multi-phase analysis of steel-air-slag system during ladle change-over process in CC tundish steelmaking process. In Proceedings of the Asia Steel International Conference, Yokohama, Japan, 5–8 October 2015.
14. Youngs, D.L. Time-dependent multi-material flow with large fluid distortion. In *Numerical Methods in Fluid Dynamics*; Morton, K.W., Baines, M.J., Eds.; Academic Press: Cambridge, MA, USA, 1982; pp. 273–285.
15. Odenthal, H.J.; Bölling, R.; Pfeifer, H. Three-dimensional LDA and DPIV investigations of tundish water models. In Proceedings of the 2nd International Conference on the Science & Technology of Steelmaking, Swansea, UK, 10–11 April 2001; pp. 499–517.
16. Sahai, Y.; Emi, T. Physical modeling of melt flow in continuous casting tundishes. In Proceedings of the International Conference on Modelling and Simulation in Metallurgical Engineering and Materials Science, Beijing, China, 11–13 June 1996.



© 2018 by the authors. Licensee MDPI, Basel, Switzerland. This article is an open access article distributed under the terms and conditions of the Creative Commons Attribution (CC BY) license (<http://creativecommons.org/licenses/by/4.0/>).